A Letters Journal Exploring the Frontiers of Physics

December 2009

EPL, **88** (2009) 65001 www.epljournal.org
doi: 10.1209/0295-5075/88/65001

Measurements of the power spectrum and dispersion relation of self-excited dust acoustic waves

V. Nosenko[1(a)], S. K. Zhdanov[1], S.-H. Kim[2], J. Heinrich[2], R. L. Merlino[2] and G. E. Morfill[1]

[1] *Max-Planck-Institut für extraterrestrische Physik - D-85741 Garching, Germany, EU*
[2] *Department of Physics and Astronomy, The University of Iowa - Iowa City, IA 52242, USA*

received 1 September 2009; accepted in final form 25 November 2009
published online 4 January 2010

PACS 52.27.Lw – Dusty or complex plasmas; plasma crystals
PACS 52.27.Gr – Strongly-coupled plasmas
PACS 52.35.Fp – Electrostatic waves and oscillations (*e.g.*, ion-acoustic waves)

Abstract – The spectrum of spontaneously excited dust acoustic waves was measured. The waves were observed with high temporal resolution using a fast video camera operating at 1000 frames per second. The experimental system was a suspension of micron-size kaolin particles in the anode region of a dc discharge in argon. Wave activity was found at frequencies as high as 450 Hz. At high wave numbers, the wave dispersion relation was acoustic-like (frequency proportional to wave number). At low wave numbers, the wave frequency did not tend to zero, but reached a cutoff frequency instead. The cutoff value declined with distance from the anode. We ascribe the observed cutoff to the particle confinement in this region.

Introduction. – The dispersion relation (*i.e.*, wave frequency as a function of wave number) and the spectral energy distribution of a given wave mode contain a great deal of information on the basic physics of the system in question. Of particular interest is the long-wavelength/low-frequency limit of the dispersion relation. Here, the wave frequency ω can tend to zero for wave numbers $k \to 0$ (which is a characteristic of different kinds of sound waves), or various cutoffs can exist, for example $\omega \to \omega_c$ for $k \to 0$, where ω_c is a finite value. Examples of waves with a frequency cutoff are sound waves in ducts [1], Langmuir waves in plasmas, electromagnetic waves at the critical plasma density [2], and waves in magnetic flux tubes on the Sun [3]. The physics of frequency cutoff is different in these examples, but it can be vaguely described as a confinement at that frequency.

Complex (dusty) plasmas are excellent model systems to study wave phenomena down to the level of individual "atoms" [4–9]. A complex or dusty plasma is a multicomponent system of ionized gas and solid microparticles, with sizes typically in range of tens of nanometers to tens of micrometers [10,11]. The solid microparticles acquire an electric charge by the attachment of electrons and ions. In typical laboratory dusty plasmas, the thermal speed of the electrons is considerably higher than that of the positive ions, so the microparticle charge is negative. When the charge density of the microparticles is not much smaller than the charge density of the ions, the microparticles exhibit collective behavior and various wave modes can be sustained in the complex plasma.

One of the most well-studied wave mode is the dust acoustic wave [12] (DAW) where the inertia is provided by massive dust grains and the restoring force is provided by the electrostatic pressure due to electrons and ions. The dust acoustic wave was first observed by Chu, Du, and I [13] and by Barkan, Merlino and D'Angelo [4]. Subsequently, the DAW has been studied by many groups in a variety of dusty plasmas, in both ground-based laboratories as well as under microgravity conditions [14–20]. The dispersion relation of the DAW was calculated theoretically using fluid [12] and kinetic [21] approaches, and also measured experimentally by external modulation of the wave frequency [22–27].

The behavior of DAW in the long-wavelength/low-frequency limit is of particular interest. A *wave number cutoff*, that is a finite wave number k_c at $\omega \to 0$ was predicted in refs. [28,29] based on the notion of attractive forces between dust grains (*e.g.*, due to the ion shadowing effect). A similar wave number cutoff for self-excited DAW can also arise due to dust-neutral collisions [5]. Previous measurements were not able to resolve these features in the DAW dispersion relation. On the other hand, a *frequency*

(a) E-mail: nosenko@mpe.mpg.de

cutoff, that is a finite frequency ω_c as $k \to 0$ was predicted theoretically [30,31] and reported in an experiment [32] where DAW were externally excited in the frequency range of 17–30 Hz.

In this paper, we present the first experimental measurement of the power spectrum and dispersion relation of self-excited dust acoustic waves using high speed video imaging and Fourier analysis techniques. A DAW spectrum with frequencies extending up to ≈500 Hz was observed. The dispersion relation continues to be acoustic-like ($\omega \propto k$) at high frequencies and has a low-frequency cutoff at low wave numbers. A dust-ion streaming instability is the most likely mechanism for the spontaneously excited waves [33,34].

Experimental method. – Our experimental system was a suspension of fine kaolin microparticles in the anode region of a dc discharge in argon [5]. The vacuum chamber is a horizontal stainless steel cylinder with a diameter of 60 cm and length of 90 cm. The anode is a steel disk with a diameter of 3 cm located at the chamber axis, the cathode is the inside surface of the (grounded) vacuum chamber. External coils provide axial magnetic field. Below the anode, there is an electrically floating tray with kaolin powder. The plasma chamber is equipped with a planar Langmuir probe that can be moved along the chamber axis.

The experimental parameters were as follows. We used Ar at a pressure of 78–200 mtorr. The discharge current could be varied in the range of 5–20 mA. The longitudinal magnetic field was about 100 G. We used polydisperse kaolin microparticles with average size of 1 μm and mass $\approx 10^{-15}$ kg [24]. The neutral-gas damping rate was in the range of $\nu_{\mathrm{E}} = 90$–$240\,\mathrm{s}^{-1}$, as modeled [35] by the Epstein expression.

After the discharge was switched on, the particles started to jump from the tray up into the anode fall region of the discharge. After around 30 min, a cylindrically shaped particle cloud was formed with a diameter of ≈3 cm and length of ≈5 cm. We visualized a vertical cross-section of the cloud by illuminating the particles with a vertical sheet of laser light ($\lambda = 532$ nm) and imaging them with a side-view camera. We used the Photron FASTCAM 1024PCI camera that has a spatial resolution of $1024 \times 1024\,\mathrm{pixels}^2$ and operated at the rate of 1000 frames per second.

In a wide range of experimental parameters, dust acoustic waves were spontaneously excited in the particle cloud [5], probably due to an ion-dust streaming instability [21]. The waves were readily seen by the side-view camera as spatio-temporal variations of the intensity of laser light scattered off particles caused by periodic modulations of the particle number density. A snapshot of these waves is shown in fig. 1(a).

To analyze the wave propagation, we produced space-time plots of their intensity, shown in fig. 1(b), based on

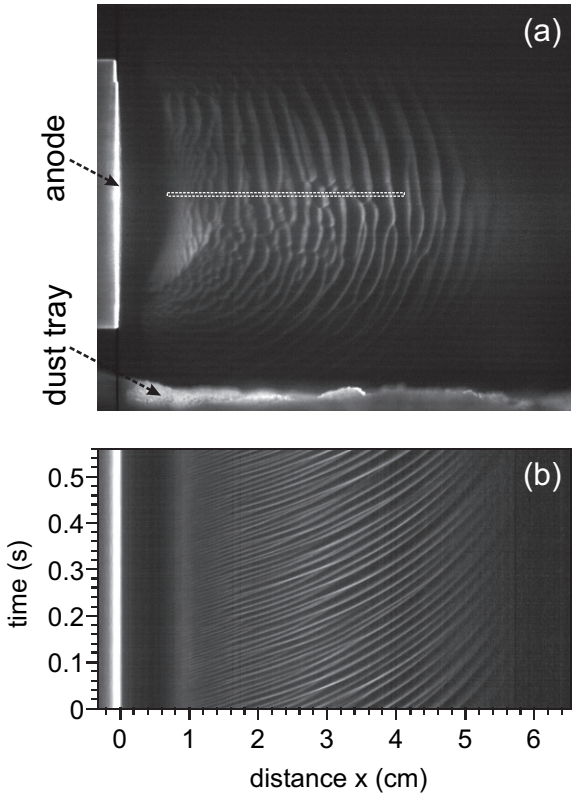

Fig. 1: Spontaneously excited dust acoustic waves (DAW). Shown are (a) a snapshot of DAW and (b) space-time plot of the DAW image intensity. Micron-size kaolin particles are levitated in the anode region of a dc discharge in argon at 124 mtorr. The dotted-line rectangle in (a) corresponds to the "wide analysis area".

images like that in fig. 1(a). As seen from the upward curvature of the bright features in fig. 1(b), the wave speed drops significantly with distance from the anode. Therefore, we perform our analysis separately at different distances x. First, we restrict our analysis to the region where the wave speed does not change much ($x =$ 0.68–4.11 cm, shown in fig. 1(a)). Below, we call this "wide analysis area". Then, we repeat our analysis in six smaller adjacent regions; this gives the dependence of wave parameters on the distance from the anode.

The dispersion relation of DAW was calculated using the following method. We start with the pixel intensity of raw experimental images of waves $I(x, y, t)$. We assume that $I(x, y, t)$ is proportional to the intensity of laser light scattered off dust grains, which in turn is proportional to the local number density of dust grains. The first assumption is based on camera's $\gamma = 1$ (pixel intensity proportional to incoming light intensity), the second assumption was supported in ref. [34].

We averaged the pixel intensity $I(x, y, t)$ over all values of y in a narrow rectangular region shown in fig. 1(a), to arrive at $\tilde{I}(x, t)$. Then, we performed a Fourier transform of $\tilde{I}(x, t)$ in space and time domains. The resulting

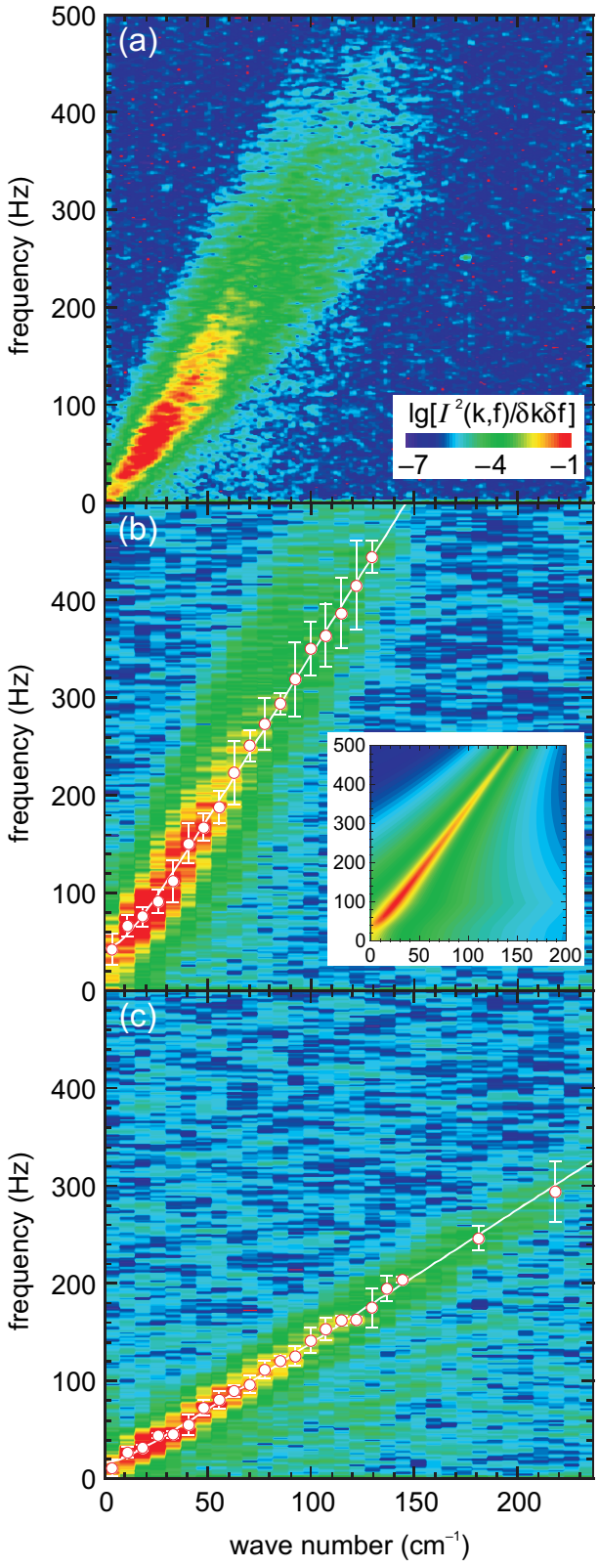

Fig. 2: (Color online) Fluctuation spectra $\mathcal{I}^2(k, f)$ of DAW image intensity for experimental conditions of fig. 1, measured at different distances from the anode: (a) 0.68–4.11 cm, (b) 1.54–2.39 cm, (c) 4.11–4.96 cm. White fit lines give the wave dispersion relation, as explained in the text. The inset in (b) shows the theoretically calculated wave spectrum.

fluctuation spectrum $\mathcal{I}^2(k, f)$, fig. 2, gives the map of DAW energy in the wave number - frequency space. Note that our method is similar to that of refs. [6,9,36], where particle velocities from a computer simulation [36] or an experiment [6,9] were used as input for the Fourier transform. The fit lines in figs. 2(b), (c) give the wave dispersion relations, as we explain later in the text.

Results and discussion. – The dispersion relations calculated in the wide analysis area appear to be acoustic-like (frequency proportional to wave number), in the entire range of frequencies where the waves were spontaneously excited. A typical example is shown in fig. 2(a). Note that the wave activity is present at frequencies as high as 400 Hz. There are no waves above approximately 450 Hz. This means that the frame rate of 1000 frames per second was chosen adequately (the Nyquist frequency is 500 Hz); using a lower frame rate would lead to aliasing in the frequency domain that would distort the calculated dispersion relations.

The wave energy is distributed unequally between different wave numbers, as seen in fig. 2(a). The wave power spectrum has a maximum at approximately 20–30 cm^{-1}. This agrees with the kinetic calculations of ref. [25] where a positive growth rate for DAW was reported with a maximum at the wave number of $k_{\max} \approx 0.4/\lambda_{Di}$. In our experiment, $\lambda_{Di} \approx 0.014$ cm, giving $k_{\max} \approx 30\,\mathrm{cm}^{-1}$ or corresponding wavelength ≈ 0.2 cm.

In the wide analysis area, the acoustic-like behavior apparently extends to low frequencies. In particular, no wave number cutoff is seen in our experimental dispersion relation in fig. 2(a). Predicted values of the wave number cutoff should be in the range of 3–11 cm^{-1} in our experimental conditions according to ref. [28], for dust temperature in the range of 0.025–25 eV. The wave number cutoff due to neutral-dust collisions should be around $\nu_{\mathrm{E}}/2C_s \approx 3\,\mathrm{cm}^{-1}$ for the conditions of fig. 2. In principle these cutoffs should be observable in our current experiment. This would give us the possibility to actually measure the attractive component of the binary-interaction potential between the microparticles.

The slope of the dispersion relation gives the wave speed C_{DAW}. We plotted the dispersion relations like that shown in fig. 2(a) for all combinations of the gas pressure and discharge current where spontaneously excited DAW were present. They all have a similar shape, only the slope is different. From these, we calculated C_{DAW} as a function of the gas pressure and discharge current. It varies from 16 cm/s to 29 cm/s, C_{DAW} being lower for higher pressures of argon in the explored range of 78–200 mtorr.

This can be due to the following three possible causes. First, C_{DAW} is directly proportional to the particle charge Q. Q, in turn, depends on the electron temperature T_e, which decreases with increasing pressure. Second, C_{DAW} also depends on the dust temperature T_d, which decreases with increasing pressure [37]. Third, the real

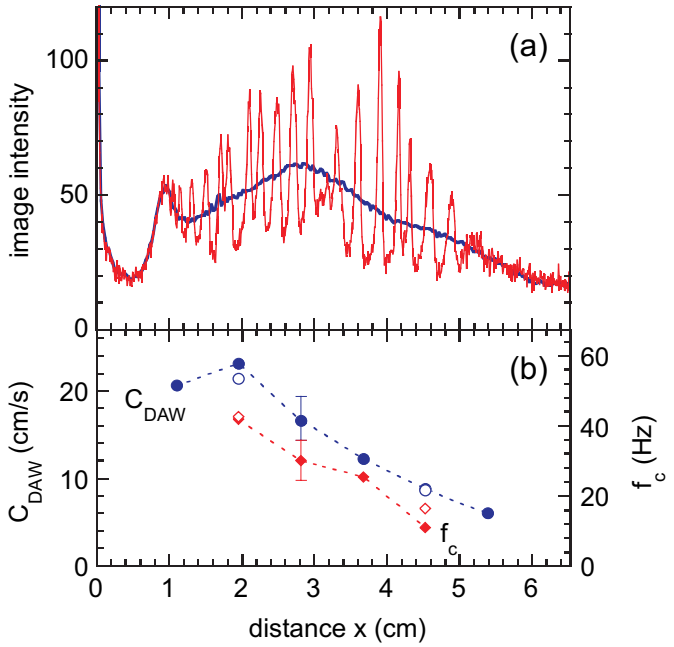

Fig. 3: (Color online) (a) Snapshot of DAW (thin line) and time-averaged image intensity (bold line). (b) Wave speed C_{DAW} (circles) and the frequency cutoff f_c (diamonds) are shown as a function of distance from the anode. Open symbols are calculated from the fits in figs. 2(b), (c). Solid symbols for C_{DAW} and f_c are calculated, respectively, from the slope of the $f \propto k$ feature in $\mathcal{I}^2(k,f)$ and the Gaussian fit of $\mathcal{I}^2(k_{\min},f)$.

part of the dispersion relation including the effects of dust-neutral collisions shows that the phase speed decreases with the gas damping rate ν_{E}, which is proportional to pressure. This latter mechanism, however, does not play a significant role in our experiment. The discharge current does not seem to have any systematic effect on C_{DAW}.

The speed of waves declines as they travel away from the anode. This can be seen from the corresponding upward curvature of the wave space-time plot in fig. 1(b). This also leads to the broadening of the wave spectrum in fig. 2(a), as different wave speeds at different distances x from the anode are factored in.

To study C_{DAW} as a function of x, we divided the region where DAW were present into six smaller adjacent windows each 0.86 cm wide. Then we calculated the wave spectra separately in each window. Two of these are shown in figs. 2(b),(c), measured close to the anode and far from it, respectively. C_{DAW} is indeed significantly lower far from the anode. The dependence $C_{\mathrm{DAW}}(x)$ is shown in fig. 3(b). There is a correlation between $C_{\mathrm{DAW}}(x)$ and the average dust number density (represented by the average pixel intensity of wave images, fig. 3(a)) for $x \geqslant 2.8$ cm, but not for $x < 2.8$ cm.

A remarkable feature of the dispersion relation measured near the anode, fig. 2(b), is a frequency cutoff at low wave numbers. Indeed, the wave frequency does not tend to zero for $k \to 0$, but reaches a finite cutoff frequency f_c instead. The white circles in fig. 2(b) are calculated as the maxima of the wave power spectrum w.r.t. frequency, for every value of wave number. The white curve is a fit with $f = \sqrt{(C_{\mathrm{DAW}}/2\pi)^2 k^2 + f_c^2}$, where C_{DAW} and f_c are fit parameters. Far from the anode, the frequency cutoff is much lower and difficult to resolve, as seen in fig. 2(c). A simpler method to measure C_{DAW} and f_c is to calculate, respectively, the slope of the $f \propto k$ feature in $\mathcal{I}^2(k,f)$ and the frequency where $\mathcal{I}^2(k_{\min},f)$ has its maximum ($k_{\min}$ is the minimum wave number). Both methods give similar results, as shown in fig. 3(b), therefore, below we use the simpler method.

The value of frequency cutoff declines with distance from the anode, as shown in fig. 3(b). The gradient length for f_c is similar to that for C_{DAW}. When power spectra from different locations are combined, as in fig. 2(a), the frequency cutoff becomes undetectable.

Model of frequency cutoff. – We ascribe the observed frequency cutoff to the particle confinement near the anode. Two kinds of confinement may be involved: radial and axial. The role of (radial) boundary effects on the dispersion relation of DAW was discussed in ref. [30]. The axial inhomogeneity (confinement) of dust particle suspensions in anodic plasmas was discussed in ref. [26].

We propose a simple model of the frequency cutoff that is a natural extension of the model of ref. [30] to empirically take different kinds of confinement into account. Let us assume that the waves are driven from the anode side (at $x = 0$). Then near the anode the dynamics of the dust number density n is governed by the following fluid equation: $n_{tt} + \nu_{\mathrm{E}} n_t - C_{\mathrm{DAW}}^2 n_{xx} = -\omega_0^2 n$ with the boundary condition $n|_{x=0} = f(\omega)\exp(-i\omega t)$. Here, ω_0 is the confinement frequency that characterizes confinement strength and $f(\omega)$ is the excitation spectral density.

Wave spectra produced by our model are similar to those observed experimentally, as shown in fig. 2(b) and in the inset. The main features of the experimental spectra are reproduced including the frequency cutoff $f_c = (2\pi)^{-1}\sqrt{\omega_0^2 - \nu_{\mathrm{E}}^2/4}$. In the calculation, we used $f(\omega) = 1$ for $\omega \leqslant \Delta\omega$ and $f(\omega) = \exp[-(\omega - \Delta\omega)\tau]$ otherwise, where $\Delta\omega = 0.4 C_{\mathrm{DAW}}/\lambda_{Di}$ and $\tau = \lambda_{Di}/C_{\mathrm{DAW}}$. The confinement strength ω_0 was a fit parameter, all other parameters were chosen as in the experiment.

Another notable feature of our model is that it predicts either frequency or wave number cutoff depending on the neutral-gas friction rate. The frequency cutoff is present only if the gas damping rate is sufficiently low, so that $2\omega_0/\nu_{\mathrm{E}} > 1$. For example, in the experimental conditions of fig. 2(b), $2\omega_0/\nu_{\mathrm{E}} \approx 3.4$.

Our model empirically takes the particle confinement into account without specifying the exact type of confinement. The role of (radial) boundary effects on the dispersion relation of DAW was first discussed in ref. [30]. Our model recovers the dispersion relation obtained in ref. [30]

for $\nu_{\rm E} \ll \omega_{pd}$ and $\omega_0 \equiv \gamma_n \omega_{pd} \lambda_D / R$, where γ_n is the root of the Bessel function J_0 and R is the anode radius. For the geometry of our experiment, $\gamma_n = \gamma_1 \cong 2.4$, the resulting cutoff frequency is about $f_c \approx 10\,\text{Hz}$. This value is consistent with our measurement far from the anode, as shown in fig. 3(b). However, near the anode the cutoff value is substantially higher, around 42 Hz. We propose that axial confinement of particles [26] is responsible for the enhanced frequency cutoff near the anode.

Note that the proposed model is based on a linear fluid equation, whereas the waves in our experiment grow from low amplitude near the anode to large amplitude in the bulk of the particle suspension, see fig. 3(a). The observed frequency cutoff is the most conspicuous near the anode, where the waves are low-amplitude and probably linear; here, our model should be directly applicable as indicated by good agreement between the model and experimental measurement, fig. 2(b). The effect of particle confinement may then carry to the nonlinear stage of the wave development.

Summary and conclusions. – To summarize, the dispersion relation of dust acoustic waves was measured in a wide frequency range. A frequency cutoff was observed, *i.e.* the long-wavelength waves had a finite non-zero frequency. We propose a simple model that explains this observation by particle confinement in plasma. The existence of a cutoff frequency is very important for the propagation of waves: the waves excited above the cutoff are propagating, and those below cutoff are evanescent. Future experiments to determine the attractive part of the binary-interaction potential [28,29] from DAW have to be conducted without confinements as this masks those effects.

* * *

We thank A. V. Ivlev for helpful discussions. The work at the University of Iowa was supported by the U.S. Department of Energy Grant No. DE-FG02-04ER54795.

REFERENCES

[1] Morse P. M. and Ingard K. U., *Theoretical Acoustics* (McGraw-Hill, NY) 1968.
[2] Nishikawa K. and Wakatani M., *Plasma Physics: Basic Theory with Fusion Applications*, 3rd edition (Springer-Verlag, Berlin) 2000.
[3] Spruit H. C. and Roberts B., *Nature (London)*, **304** (1983) 401.
[4] Barkan A., Merlino R. L. and D'Angelo N., *Phys. Plasmas*, **2** (1995) 3563.
[5] Merlino R. L., Barkan A., Thompson C. and D'Angelo N., *Phys. Plasmas*, **5** (1998) 1607.
[6] Nunomura S., Goree J., Hu S., Wang X., Bhattacharjee A. and Avinash K., *Phys. Rev. Lett.*, **89** (2002) 035001.
[7] Piel A., Homann A., Klindworth M., Melzer A., Zafiu C., Nosenko V. and Goree J., *J. Phys. B*, **36** (2003) 533.
[8] Nosenko V., Goree J. and Skiff F., *Phys. Rev. E*, **73** (2006) 016401.
[9] Nosenko V., Goree J. and Piel A., *Phys. Rev. Lett.*, **97** (2006) 115001.
[10] Shukla P. K. and Mamun A. A., *Introduction to Dusty Plasma Physics* (IOP Publ., Bristol) 2001.
[11] Fortov V. E., Ivlev A. V., Khrapak S. A., Khrapak A. G. and Morfill G. E., *Phys. Rep.*, **421** (2005) 1.
[12] Rao N. N., Shukla P. K. and Yu M. Y., *Planet. Space Sci.*, **38** (1990) 543.
[13] Chu J. H., Du J. B. and Lin I., *J. Phys. D: Appl. Phys.*, **27** (1994) 296; D'Angelo N., *J. Phys. D: Appl. Phys.*, **28** (1995) 1009.
[14] Prabhakara H. R. and Tanna V. L., *Phys. Plasmas*, **3** (1996) 3176.
[15] Molotkov V. I., Nefedov A. P., Torchinski V. M., Fortov V. E. and Khrapak A. G. , *J. Exp. Theor. Phys.*, **89** (1999) 477.
[16] Fortov V. E., Khrapak A. G., Khrapak S. A., Molotkov V. I., Nefedov A. P., Petrov O. F. and Torchinski V. M., *Phys. Plasmas*, **7** (2000) 1374.
[17] Fortov V. E., Usachev A. D., Zobnin A. V., Molotkov V. I. and Petrov O. F., *Phys. Plasmas*, **10** (2003) 1199.
[18] Pramanik J., Veeresha B. M., Prasad G., Sen A. and Kaw P. K., *Phys. Lett. A*, **312** (2003) 84.
[19] Piel A., Klindworth M. and Arp O., *Phys. Rev. Lett.*, **97** (2006) 205009.
[20] Schwabe M., Rubin-Zuzic M., Zhdanov S., Thomas H. M. and Morfill G. E., *Phys. Rev. Lett.*, **99** (2007) 095002.
[21] Rosenberg M., *Planet. Space Sci.*, **41** (1993) 229.
[22] Williams J. D., Thomas E. jr. and Marcus L., *Phys. Plasmas*, **15** (2008) 043704.
[23] Annibaldi S. V., Ivlev A. V., Konopka U., Ratunskaia S., Thomas H. M., Morfill G. E., Lipaev A. M., Molotkov V. I., Petrov O. F. and Fortov V. E., *New J. Phys.*, **9** (2007) 321.
[24] Thompson C., Barkan A., D'Angelo N. and Merlino R. L., *Phys. Plasmas*, **4** (1997) 2331.
[25] Rosenberg M., Thomas E. Jr. and Merlino R. L., *Phys. Plasmas*, **15** (2008) 073701.
[26] Trottenberg T., Block D. and Piel A., *Phys. Plasmas*, **13** (2006) 042105.
[27] Thomas E. Jr., Fisher R. and Merlino R. L., *Phys. Plasmas*, **14** (2007) 123701.
[28] Tsytovich V. N., *Phys. Scr.*, **74** (2006) C81.
[29] Tsytovich V. and Morfill G., *Contrib. Plasma Phys.*, **47** (2007) 157.
[30] Shukla P. K. and Rosenberg M., *Phys. Plasmas*, **6** (1999) 1038.
[31] Yaroshenko V. V., Thomas H. M. and Morfill G. E., *Phys. Plasmas*, **14** (2007) 082104.
[32] Pilch I., Piel A., Trottenberg T. and Koepke M. E., *Phys. Plasmas*, **14** (2007) 123704.
[33] D'Angelo N. and Merlino R. L., *Planet. Space Sci.*, **44** (1996) 1593; Rosenberg M., *J. Vac. Sci. Technol. A*, **14** (1996) 631; Kaw P. and Singh R., *Phys. Rev. Lett.*, **79** (1997) 423; Fortov V. E., Khrapak A. G., Khrapak S. A., Molokov V. I., Nefedov A. P., Petrov O. F. and Torchinsky

V. M., *Phys. Plasmas*, **7** (2000) 1374; Ostrikov K. N., Vladimirov S. V., Yu M. Y. and Morfill G. E., *Phys. Rev. E*, **61** (2000) 4315; Ivlev A. V., Samsonov D., Goree J. and Morfill G., *Phys. Plasmas*, **6** (1999) 741; Rosenberg M., *J. Plasma Phys.*, **67** (2002) 2350242.

[34] Schwabe M., Zhdanov S. K., Thomas H. M., Ivlev A. V., Rubin-Zuzic M., Morfill G. E., Molotkov V. I., Lipaev A. M., Fortov V. E. and Reiter T., *New J. Phys.*, **10** (2008) 033037.

[35] Liu B., Goree J. and Nosenko V., *Phys. Plasmas*, **10** (2003) 9.

[36] Schmidt P., Zwicknagel G., Reinhard P.-G. and Toepffer C., *Phys. Rev. E*, **56** (1997) 7310.

[37] Thomas H. M. and Morfill G. E., *Nature (London)*, **379** (1996) 806.